plasma

MDPI

Article

Tailoring Black TiO_2 Thin Films: Insights from Hollow Cathode Hydrogen Plasma Treatment Duration

Armstrong Godoy-Junior [1,*], André Pereira [1], Barbara Damasceno [1], Isabela Horta [1], Marcilene Gomes [2], Douglas Leite [1], Walter Miyakawa [3], Maurício Baldan [4], Marcos Massi [5], Rodrigo Pessoa [1,*] and Argemiro da Silva Sobrinho [1,*]

[1] Laboratório de Plasmas e Processos (LPP), Instituto Tecnológico de Aeronáutica (ITA), Praça Mal. Eduardo Gomes, 50, São José dos Campos 12228-900, SP, Brazil; andreljpereira@gmail.com (A.P.); barbdara@gmail.com (B.D.); isabelah1@poli.ufrj.br (I.H.); leite@ita.br (D.L.)
[2] Instituto Federal de Educação, Ciência e Tecnologia de São Paulo (IFSP), Rod. Pres. Dutra, km 145, São José dos Campos 12223-201, SP, Brazil; marcilenecgomes@ifsp.edu.br
[3] Instituto de Estudos Avançados (IEAv), Trevo Coronel Aviador José Alberto Albano do Amarante, 1, São José dos Campos 12228-001, SP, Brazil; walter.toshi@gmail.com
[4] Instituto Nacional de Pesquisas Espaciais (INPE), Av. dos Astronautas, 1758, Jardim da Granja, São José dos Campos 12227-010, SP, Brazil; mrbaldan@gmail.com
[5] Escola de Engenharia, Universidade Presbiteriana Mackenzie, Consolação, 930, São Paulo 01302-907, SP, Brazil; massi.marcos@gmail.com
* Correspondence: godoyajr@gmail.com (A.G.-J.); rspessoa@ita.br (R.P.); argemiro@ita.br (A.d.S.S.)

Abstract: In this study, we report the use of a radiofrequency plasma-assisted chemical vapor deposition (RF-CVD) system with a hollow cathode geometry to hydrogenate anatase TiO_2 thin films. The goal was to create black TiO_2 films with improved light absorption capabilities. The initial TiO_2 was developed through magnetron sputtering, and this study specifically investigated the impact of hollow cathode *hydrogen plasma* (HCHP) treatment duration on the crucial characteristics of the resulting black TiO_2 films. The HCHP treatment effectively created in-bandgap states in the TiO_2 structure, leading to enhanced light absorption and improved conductivity. Morphological analysis showed a 24% surface area increase after 15 min of treatment. Wettability and surface energy results displayed nonlinear behavior, highlighting the influence of morphology on hydrophilicity improvement. The anatase TiO_2 phase remained consistent, as confirmed by diffractograms. Raman analysis revealed structural alterations and induced lattice defects. Treated samples exhibited outstanding photodegradation performance, removing over 45% of methylene blue dye compared to ~25% by the pristine TiO_2 film. The study emphasized the significant impact of 15-min hydrogenation on the HCHP treatment. The research provided valuable insights into the role of hydrogenation time using the HCHP treatment route on anatase TiO_2 thin films and demonstrated the potential of the produced black TiO_2 thin films for photocatalytic applications.

Keywords: black TiO_2; hollow cathode; *hydrogen plasma*; hydrogenation; photocatalysis

Citation: Godoy-Junior, A.; Pereira, A.; Damasceno, B.; Horta, I.; Gomes, M.; Leite, D.; Miyakawa, W.; Baldan, M.; Massi, M.; Pessoa, R.; et al. Tailoring Black TiO_2 Thin Films: Insights from Hollow Cathode Hydrogen Plasma Treatment Duration. *Plasma* **2023**, *6*, 362–378. https://doi.org/10.3390/plasma6020025

Academic Editor: Andrey Starikovskiy

Received: 4 May 2023
Revised: 26 May 2023
Accepted: 30 May 2023
Published: 1 June 2023

1. Introduction

Nowadays, semiconductor materials have been extensively researched as they form the foundation for a wide range of electronic and optoelectronic devices that can be applied in sectors focused on addressing environmental and energy challenges [1–3]. In the context of technologies such as solar cells, hydrogen production, or water purification, a desirable characteristic for the application of semiconductors is the absorption of all sunlight radiation, or at least most of it, that reaches the Earth [4]. This presents a challenge, as many of the semiconductor-based materials used for these purposes typically possess wide bandgaps, which do not permit the absorption of the entire solar spectrum, encompassing the ultraviolet (UV), visible (Vis), and near-infrared (NIR) ranges [5]. Consequently, numerous researchers have been devoted to the modification of these materials to enhance

their optoelectronic properties, aiming for maximum absorption of radiation in the visible region [6–8].

In 2011, Chen et al. published a study on a novel structural modification conducted on pristine TiO_2 nanoparticles (NPs) [6]. They reported that this newly modified TiO_2, termed "black TiO_2", was capable of absorbing electromagnetic radiation from the UV to the NIR range. This enhanced absorption was a result of the bandgap narrowing from 3.3 eV (pristine anatase TiO_2) to 1.54 eV (black TiO_2), achieved after heat treatment in a hydrogen atmosphere under high pressure using a Hy-Energy Pressure–Composition Isotherm (PCTPro) [6]. This hydrogenation process induced the creation of defects and structural disorder in the TiO_2 NPs, facilitated by the incorporation of hydrogen and the removal of oxygen atoms. This was responsible for the bandgap narrowing and the subsequent increase in light absorption [6].

Considering the extreme experimental conditions employed by Chen et al., such as high hydrogen pressure (a flammable gas) and lengthy process times, numerous studies have since been conducted with proposals to optimize the hydrogenation methodology [9,10]. The primary expected characteristics of black TiO_2 include bandgap narrowing, the creation of Ti^{3+}/Ti^{2+} oxidation states, oxygen vacancies (V_o), microstructural disorder, increased surface area, presence of OH groups on the surface, in-gap states, and enhanced absorption of visible light [11]. To date, the most used methods are based on laser processes [12], plasma-assisted treatments [13], chemical reductions [14], and low-/high-pressure heat treatments [15–17]. Among these, plasma-based processes have been employed through various configurations: thermal plasma furnaces [18], non-thermal dielectric barrier discharges (DBD) [19], plasma sprays [20,21], chemical vapor deposition (CVD) [22,23], and others [13,24]. In this context, the CVD method is one of the most promising for synthesizing black TiO_2, primarily due to its relatively mild conditions (low pressure and short processing time) and the intense chemical reactions that this technique offers without damaging the material's internal microstructure.

Numerous studies have reported black TiO_2 NPs treated under a hydrogen atmosphere and subsequently applied in various fields, such as lithium-ion batteries [25], photocatalysis [26], photothermal cancer therapy [27], and others. In contrast, only a few studies have explored the use of black TiO_2 in thin-film form as a potential alternative for enhancing photocatalytic activity [22,23].

Black TiO_2 thin films offer several advantages compared to black TiO_2 NPs as their morphology provides improved performance when applied to solar cells and photocatalytic treatments. Furthermore, their form allows for the easy reuse of the same thin film, minimizing secondary residues in the natural environment where photocatalysis is performed, which may not be the case when using powders.

Recently, an RF-CVD system integrated with an HCHP setup was employed for hydrogenating anatase TiO_2 thin films [11]. This method proved to be swift and effective, producing black TiO_2 thin films with enhanced solar light absorption in a short processing duration, thus showing promise as a photocatalyst for pollutant degradation [11]. The current study builds upon these findings, exploring the impact of HCHP processing time on the properties and photocatalytic activity of black TiO_2 thin films. In this experiment, pristine anatase TiO_2 thin films were subjected to HCHP treatment for varying treatment times (15, 30, 45, and 60 min) under controlled plasma parameters. Post-treatment, each sample was assessed, considering morphological, microstructural, chemical, optical, electrical, and wettability characteristics. This evaluation was conducted to garner a deeper understanding of how the processing time during HCHP treatment influences the overall performance of the resulting black TiO_2 thin film. The photocatalytic activity was gauged by observing the degradation of methylene blue (MB).

2. Materials and Methods

2.1. Materials

Silicon wafers and glass slides were adopted as substrates in this study. Pieces of 0.5×0.5 cm^2 p-type Si (100) were purchased from UniversityWafer Inc. (South Boston, VA, USA). Wafers of 2×2 cm^2 glass were obtained from Perfecta (ExaCta, São Paulo, Brazil). All substrate surfaces were well cleaned before use [28]. The purity degree of the titanium (*Ti*) target, even with the oxygen (O_2), argon (Ar), and hydrogen (H_2) gases used in this study (see Sections 2.2 and 2.3), was 99.999%.

2.2. Pristine Anatase TiO_2 Thin Films Growth

Pristine TiO_2 thin films 300–400 nm thick were grown onto pieces of glass and Si (100) using a DC reactive magnetron sputtering system with a circular *Ti* target (34 mm diameter) [29]. More details concerning this step can be seen in the Supplementary Materials. Following the deposition process, the TiO_2 thin films were subjected to an annealing treatment at 450 °C using an INTI FT-1200 tubular oven under atmospheric pressure for a duration of 120 min, aiming to promote the prevalence of the anatase phase. The heating and cooling rates were 10 °C min^{-1} and 2 °C min^{-1}, respectively.

2.3. Hydrogenation Process

The HCHP treatment was performed to hydrogenate the pristine anatase TiO_2 thin films using an RF-CVD system with a hollow cathode geometry, which is schematically illustrated in Figure S1. Additionally, more details concerning this setup can be found in the Supplementary Materials.

In this paper, the samples were named as: (i) (P-TiO_2), pristine TiO_2; (ii) (B-15), black TiO_2 produced after 15 min; (iii) (B-30), black TiO_2 produced after 30 min; (iv) (B-45), black TiO_2 produced after 45 min; and (v) (B-60), black TiO_2 produced after 60 min of HCHP treatment.

2.4. Thin Film Characterization

2.4.1. Morphological Analysis

A mechanical profilometer (KLA-Tencor, P-7) was used to measure the average thickness of pristine and black TiO_2 thin films. These measurements were possible by the formation of steps on a specific region of the samples during the deposition and HCHP processes. Moreover, AFM images (1 μm^2) were acquired using Shimadzu (SPM 9500J3) equipment in which the surface area of the produced thin films was determined by the Shimadzu SPM-9500 Series Version 2.4 software.

2.4.2. Crystalline Structure and Chemical Analysis

The crystalline structure of the samples was investigated using an X-ray diffractometer (PANalytical Empyrean) with Cu K_α (1.5405 Å for $K_{\alpha1}$) as a source of incident radiation using 40 kV and 40 mA. The measurements were performed from 20° to 80° (Bragg–Brentano) range with a speed of scanning of 3.2° per min using step size and time per step of 0.013° and 60 s/step, respectively. The average crystallite size was acquired from the Rietveld refinement using HighScore software [30]. Raman spectroscopy spectra in the range of 100–700 cm^{-1} (with spectral resolution lower than 1 cm^{-1}) were collected using a Horiba-Evolution Raman spectrometer equipment using a 532 nm laser as an excitation source with power < 10 mW. The XPS examination was not preceded by any sputtering processes on the surface zone of the samples. The surface chemical and molecular composition of the produced samples were investigated by the acquisition of the *Ti 2p* and O *1s* high-resolution spectra by X-ray photoelectron spectroscopy (XPS) using a Kratos Axis Ultra spectrometer with a monochromatic Al K_α ($h\nu$ = 1486.69 eV) source at 120 W. The acquired spectra were analyzed utilizing CasaXPS software, specifically version 2.1.0.1 [31]. The peaks deconvolution was carried out using a Voight line shape after subtracting a Shirley-type background.

2.4.3. Optical and Electric Analysis

The optical properties of the black TiO_2 thin films were investigated using a UV-Vis-NIR spectrophotometer (Jasco, model V-570, Tokyo, Japan). This instrument is equipped with a 150 mm integrating sphere, and transmittance measurements were conducted over a range of 190 to 2500 nm, with the incident radiation directed normally onto the samples.

Four-point probe analysis (Jandel, RM3000, Leighton Buzzard, United Kingdom) was performed to acquire the sheet resistivity from the thin films. The analysis involved applying a current of 100 µA at three distinct points on the sample, and the mean and standard deviation values of the sheet resistance were calculated based on the obtained data.

To examine the characteristics and alterations in the valence band of the produced TiO_2 thin films following the HCHP process, XPS analysis was performed within the lower energy range of 0–12 eV. For that, the same equipment described in the previous section was used.

2.4.4. Wettability and Surface Energy Analysis

Goniometry analysis was performed by measuring the contact angles between sample surface and the droplet of a polar and nonpolar liquid (deionized water and diiodomethane, respectively) using a goniometer (Ramé-Hart, Model 500-Advanced Goniometer, Succasunna, USA). The contact angles were measured in three different regions of each sample. The average values from the acquired data were used to determine the contact angle and the surface energy. Surface energy values were calculated with a software program (DROPimage Advanced, version 2.4) that uses the harmonic mean method applied to the acid-base theory.

2.4.5. Photocatalytic Activity Evaluation

The photocatalytic degradation experiments were conducted using a custom-built reactor, which was equipped with six air-cooled UV-visible germicide lamps (Osram, model HNS G13-G15T8/OF) with a power output of 15 W each. Additional information regarding the experimental setup can be found in Figure S2. The lamps emitted an irradiance of 2.2 mW cm^{-2} at the position of the sample [32,33]. It is important to note that the reference cell did not detect the main emission peak of the lamps at 250 nm, suggesting that the actual irradiance at the sample position might be higher than the reported value (refer to Figure S3).

3. Results and Discussion

3.1. Morphological Characteristics

The thickness of the thin film diminishes as the hydrogenation duration increases. In this regard, the P-TiO_2 sample exhibits the greatest thickness, approximately 342 nm, while the B-60 sample displays the least thickness at approximately 202 nm, as demonstrated in Table 1.

Table 1. Thickness and surface energy values of the TiO_2 thin films for various HCHP treatment durations.

Sample	Thickness (nm)	Surface Energy (mN/m)
P-TiO_2	342 ± 47	61.3 ± 0.4
B-15	309 ± 10	70.0 ± 0.2
B-30	291 ± 17	67.0 ± 0.2
B-45	265 ± 21	60.0 ± 0.3
B-60	202 ± 12	47.0 ± 0.4

The obtained AFM images (Figure 1) illustrate that the pristine film displays round-shaped agglomerates with an approximate average diameter of 70 nm, while the B-15 sample presents smaller grains with an average diameter of approximately 40 nm. A subtle alteration was observed in the morphological aspects for samples with treatment durations

exceeding 15 min, characterized by the emergence of some valleys and a reduction in grain size diameter.

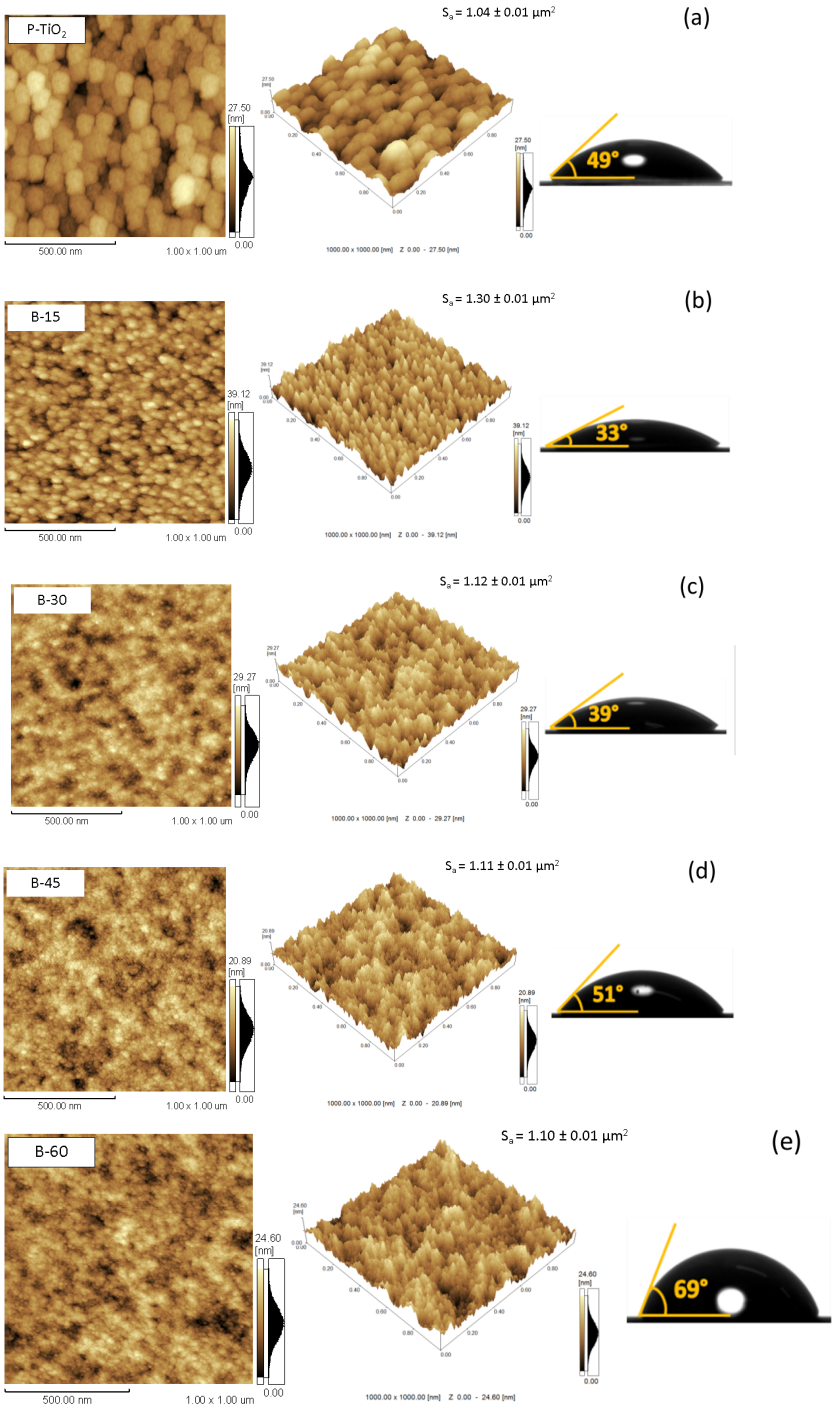

Figure 1. AFM 2D and 3D images, alongside water droplet photographs depicting the contact angles formed with the surface of (**a**) pristine and black TiO_2 films treated in the HCHP process for durations of (**b**) 15, (**c**) 30, (**d**) 45, and (**e**) 60 min. For each sample, the surface area (S_a) obtained by AFM measurements is presented.

The measured surface areas (S_a) are presented in Figure 1. The B-15 sample exhibits a higher surface area (approximately 1.30 $\pm$ 0.01 μm^2) compared to the samples treated for extended durations, which display reduced surface areas. These findings suggest that during the initial minutes of treatment, the hydrogen plasma etches the borders of the large

grains present in the pristine film, resulting in a rougher surface. However, this etching becomes detrimental for treatment durations exceeding 15 min, causing a smoothing of the film surface, consistent with the AFM results.

The etching caused by hydrogen plasma species has been previously observed in similar studies [34,35]. The authors also reported the emergence of valleys and holes resulting from the etching effect of hydrogen radicals, which can be explained by the desorption of oxygen atoms that have reacted with hydrogen radicals. Moreover, following the oxygen desorption, some *Ti* atoms may be left unbound and subsequently volatilize after absorbing sufficient energy provided by the activated hydrogen radicals from the plasma [34]. This phenomenon is particularly noticeable in this work, primarily for treatment durations exceeding 15 min, due to the employment of a hollow cathode, which renders the *hydrogen plasma* denser than in a conventional geometry, leading to more energetic hydrogen reactions with the TiO_2 surface [11].

3.2. Wettability and Surface Energy Characteristics

The contact angle measurements are presented in Figure 1. All samples exhibit hydrophilic behavior. Although the contact angle values decrease from 49° (pristine TiO_2) to 33° for brief exposure to the HCHP treatment (sample B-15), they begin to increase as the hydrogenation duration is extended, reaching 69° for the sample B-60.

As shown in Table 1, the surface energy of the produced samples follows the same trend as the water contact angles, as wettability, and consequently surface energy, depends on the chemical surface composition as well as the morphological pattern of the film surface [28,36].

The results can be attributed to the morphological pattern change observed in the sample B-15 and the significant enhancement of *OH* species concentration on its surface, which will be discussed later. Similar results were obtained by Han et al., who attributed the improvement in hydrophilic character to the presence of *OH* radicals capable of forming hydrogen bonds with water molecules [36]. However, for HCHP treatment durations longer than 15 min, we believe that the morphological changes were the primary factor in decreasing the surface energy, as we detected similar content of OH groups in the samples B-15, B-30, B-45, and B-60 (see Section 3.4) but different morphological patterns and surface area reduction after 15 min of hydrogenation. Thus, we propose that the changes observed in B-15 (the emergence of more pronounced valleys among the smaller grains) were the main contributor to the reduced hydrophilic behavior, i.e., the decrease in surface energy following 15 min of HCHP treatment.

3.3. Microstructural Characteristics

Anatase TiO_2 patterns (ICOD 01-089-4921) were observed in both the pristine and black TiO_2 sample diffractograms, as can be seen in Figure 2a. This suggests that neither the incorporation of hydrogen into the TiO_2 microstructure nor the temperature of the *hydrogen plasma* treatment (approximately 260 °C) were sufficient to significantly alter the original TiO_2 anatase tetragonal microstructure. From the XRD patterns of pristine TiO_2 and black TiO_2 films, the primary crystalline plane of anatase TiO_2 films (101) can be observed in all samples. The intensity of the (101) reflection, as well as that of other peaks, slightly decreased with increasing H doping, and the peaks shifted towards lower 2θ values, as depicted in Figure 2b. Furthermore, a decrease in the (101) peak's relative intensity can be observed, accompanied by a subtle increase in its FWHM. These changes may indicate the occurrence of stress in the films due to the *hydrogen plasma* treatment. This is attributed to lattice disorder induced by the creation of V_o, primarily because of the chemical interaction between the reactive species (H^+ and OH^- mainly) formed in the *hydrogen plasma* with the TiO_2 thin film surface [11,37] and the high kinetic energy that the hydrogen ions from the plasma impart to the film surface [38].

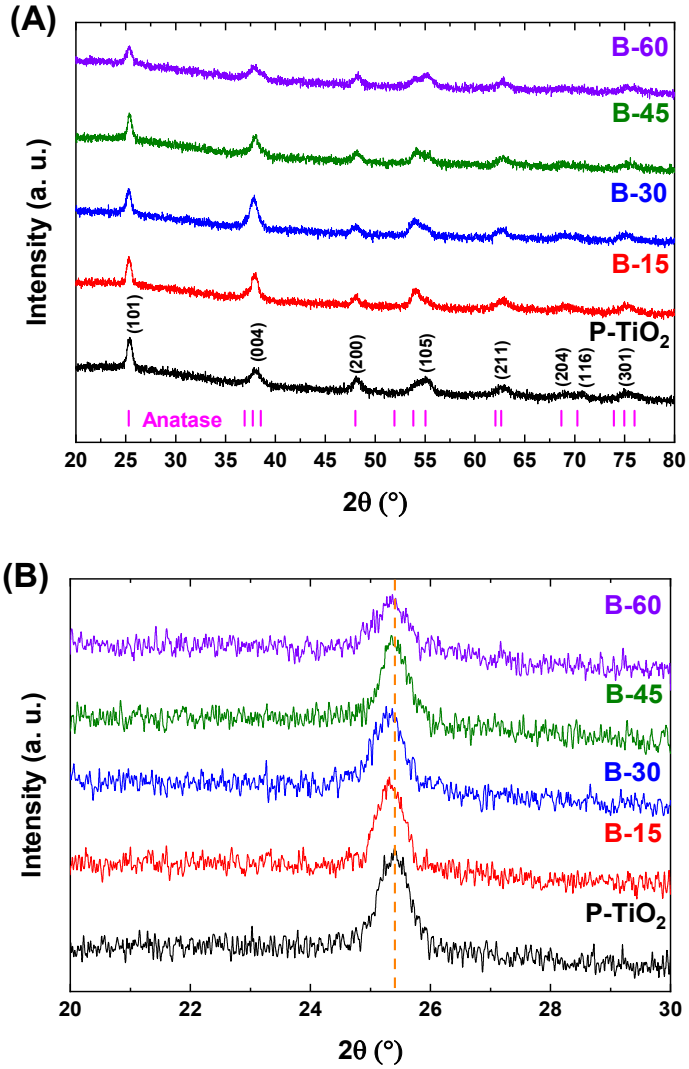

Figure 2. (**A**) TiO_2 anatase XRD patterns. (**B**) Magnified XRD patterns of (101) plane for pristine TiO_2 and B-TiO_2 thin films treated for different durations.

Furthermore, the P-TiO_2 average crystallite size was approximately (86.5 ± 7.7) Å, while the samples hydrogenated for 15, 30, and 45 min displayed an average crystallite size ranging from (89.7 ± 11.3) Å to (96.7 ± 9.0) Å. In contrast, B-60 exhibited a decrease to (73.0 ± 2.8) Å, which can be related to the previous discussion.

The reduction in average crystallite size following the hydrogenation process, as observed in the B-60 sample, may be attributed to the increase of V_o, and consequently, the lattice disorder created [39,40]. However, changes may also have occurred in the other samples, as we believe that the HCHP treatment can only hydrogenate the film's surface [11]. Considering that Cu-Kα X-rays might penetrate approximately 15 µm in depth within the samples, the changes occurring on the surface of the hydrogenated layer of the black TiO_2 thin films are obscured by the higher counts detected by the reflection of the planes corresponding to the pristine TiO_2 crystalline layer located beneath the hydrogenated layer, as depicted in Figure 3. Therefore, since B-60 likely has the thickest hydrogenated layer, the average crystallite size change was observed solely in this sample.

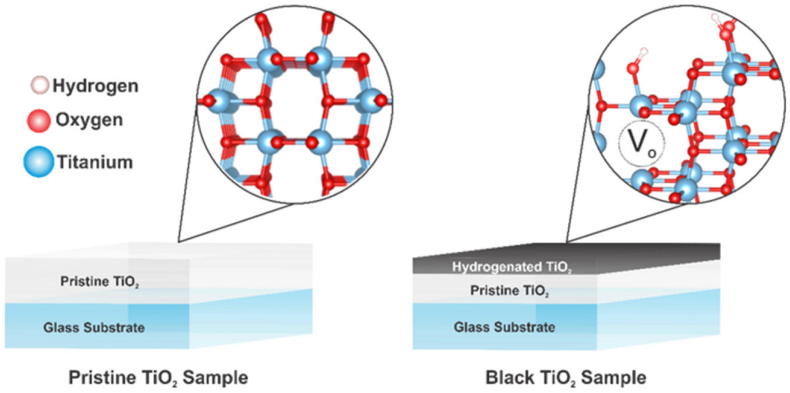

Figure 3. Schematic illustration of the pristine and black TiO_2 thin films, emphasizing their microstructures and the hydrogenated layer following HCHP treatment.

As depicted in Figure 4, micro-Raman spectroscopy analysis was conducted to evaluate the anatase TiO_2 vibrational modes. Only anatase TiO_2 vibrational modes could be detected for all samples, in agreement with the XRD results. However, by analyzing the position and profile of the main E_g anatase vibrational mode (approximately 140 cm^{-1}), some interesting behaviors could be observed.

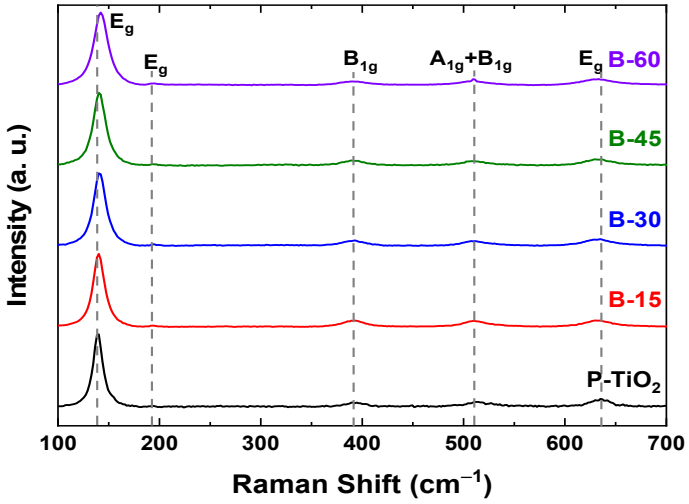

Figure 4. Raman spectra of the samples, highlighting the main anatase vibrational modes.

Table 2 demonstrates that this peak exhibits a slight blue-shift following the hydrogenation process for all samples. Additionally, a significant increase in the FWHM of this peak was observed [41]. Both blue-shift and FWHM increase of the main E_g vibrational mode detected after TiO_2 hydrogenation was also observed in previous works and is attributed to the structural changes that the TiO_2 suffers by the induced lattice defects, i.e., structural disorder promoted by the creation of V_o [16,42].

Table 2. Representation of the peak center and FWHM of the main E_g anatase vibrational mode values, along with strain variation for the chemical bonding character at different HCHP treatment durations.

Sample	E_g Peak Center (cm^{-1})	E_g FWHM (cm^{-1})
P-TiO_2	139.44	10.77
B-15	140.26	13.40
B-30	141.15	14.87
B-45	140.88	17.32
B-60	142.29	16.18

3.4. Chemical Characteristics

Surface chemical states and composition relating to each sample were investigated using XPS analysis by deconvolution of the *Ti* $2p_{3/2}$ and *O* 1*s* high-resolution spectra, as shown in Figure 5a,b, respectively.

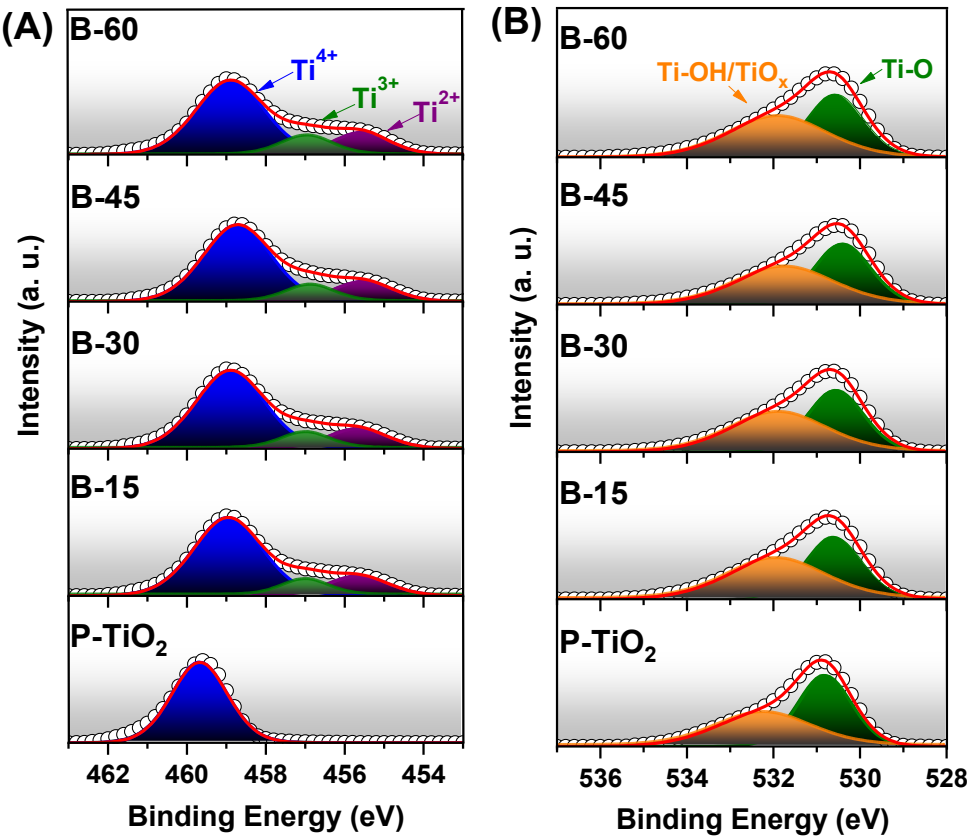

Figure 5. High-resolution XPS spectra of (**A**) *Ti* $2p_{3/2}$ and (**B**) O 1*s* peaks of each sample before and after the HCHP process during 15, 30, 45, and 60 min. Open circles and lines represent the experimental data and the fit, respectively.

The *Ti* $2p_{3/2}$ curve of the pristine sample can be deconvoluted into a single peak centered at approximately 459.7 eV, which is associated with the Ti^{4+} oxidation state [37]. The same *Ti* $2p_{3/2}$ peak undergoes a redshift of about 0.8 eV after the hydrogen treatment (B-60 sample), which can be linked to a decrease in electron density around *Ti* atoms-a strong indication that a *Ti* reduction reaction occurred during the *hydrogen plasma* treatment [43]. Indeed, the *Ti* $2p_{3/2}$ curves obtained from the black TiO_2 samples can be deconvoluted into three peaks centered at roughly 458.88 eV, 456.91 eV, and 455.54 eV, which are assigned to Ti^{4+}, Ti^{3+}, and Ti^{2+} oxidation states, respectively [36,39]. The reduction of Ti^{4+} to $Ti^{3+/2+}$ species is a consequence of the hydrogenation process through the formation of V_o [44], which were formed primarily due to the removal of oxygen atoms from the TiO_2 lattice by the creation of H_2O volatile molecules resulting from the interaction between hydrogen ions from the plasma and the oxygen atoms from the film [11,37]. The *Ti* atoms with 3+ and 2+ oxidation states, generated after the hydrogenation process, were also detected in previous studies and attributed to Ti^{3+} ions in Ti_2O_3 and Ti^{2+} ions in *TiO* [45]. Consequently, two chemical reactions are possible because of the interaction between the reactive species produced in the *hydrogen plasma* and the TiO_2 thin films during the HCHP treatment [11]:

$$2TiO_2 \xrightarrow[+2H]{\text{Hydrogen Plasma}} Ti_2O_3 + H_2O \uparrow$$

and

$$TiO_2 \xrightarrow[+H]{Hydrogen\ Plasma} TiO + H_2O \uparrow$$

It can be observed that in the presence of *hydrogen plasma*, TiO_2 might interact with H atoms, resulting in both Ti_2O_3 and/or TiO and H_2O volatile molecules. It is important to highlight that reports mainly describe the oxidation state reduction of titanium atoms after the hydrogenation process to Ti^{3+} species only [10]. However, previous studies also show Ti^{4+} reduction to *Ti* with 2+ oxidation states, besides the Ti^{3+} [36,37,40]. In general, these works reported the presence of Ti^{2+} species in its black TiO_2 mainly due to the direct reduction of Ti^{4+} oxidation states to Ti^{2+} induced by the efficient/assertive method used to induce structural defects in TiO_2. In this work, the presence of Ti^{2+} species can be related to the high density and energy of the *hydrogen plasma* generated by a hollow cathode geometry, which was able to promote the direct reduction of Ti^{4+} to Ti^{2+}.

Considering the percentage area under each curve, a significant increase (~26%) of $Ti^{3+/2+}$ species after 15 min of treatment can be noted in Table 3, but for times over 15 min, the black TiO_2 films achieve a slight increase of $Ti^{3+/2+}$ species concentration, reaching a maximum of ~30% for the sample B-60.

Table 3. XPS elemental composition in atomic percentage (at. %) and deconvolution data.

Sample	*Ti* $2p_{3/2}$	*O* 1*s*	
	$Ti^{3+/2+}$	*Ti-OH*/TiO_x	*Ti-O*
P-TiO_2	0	45.47	54.53
B-15	26.41	52.98	47.02
B-30	26.87	52.52	47.48
B-45	27.76	52.13	47.87
B-60	30.46	53.23	46.77

Concerning the O 1*s* high-resolution curve (Figure 5b), both pristine and black TiO_2 thin films can be deconvoluted into two peaks, one centered at around 532.1 eV, which may be assigned to hydroxyl groups bonded to *Ti* atoms (*Ti-OH*) or/and V_o (TiO_x) neighboring the *Ti* atoms with 3+/2+ oxidation state, and one at around 530.8 eV that may be due to *Ti-O* bindings [39,40,43]. From the acquired percentage area under each deconvoluted curve, an expressive concentration increase (from ~45% to ~53%) of hydroxyl groups/V_o on the sample B-15 and a slight variation around this value for superior treatment times can be observed in Table 3, reaching a maximum of 53% for the sample B-60. The 45% concentration for the peak centered at 532.1 eV for the pristine TiO_2 thin film can be assigned mainly to OH species from the atmosphere adsorbed on the film surface or even to intrinsic structural defects on the thin film. In Table 3, the opposite behavior for the Ti-O bonding can be observed, reaching a significant decrease for the sample B-15 (from 54.5% to 47.0%), and a slight variation around 47% for superior times.

From Table 3, an increasing behavior at a ratio of 0.25% of hydroxyl groups/oxygen vacancies and $Ti^{3+/2+}$ species concentration on the black TiO_2 thin film surface can be observed as a function of hydrogenation process time. These findings align with previous studies that have demonstrated the formation of $Ti^{3+/2+}$ species because of the generation of oxygen vacancies (V_o), as discussed earlier [37,44].

Therefore, the results obtained from the *Ti* $2p_{3/2}$ and O 1*s* deconvoluted spectra indicate that the HCHP treatment was effective in promoting both V_o and $Ti^{3+/2+}$ defects, which can narrow the bandgap of TiO_2 [6], as will be discussed further.

3.5. Optical and Electric Characteristics

The optical characteristics of the produced black TiO_2 thin films were investigated through transmittance measurements, as shown in Figure 6. The dashed line represents

the glass substrate. As expected, all samples exhibit a well-defined bandgap energy E_g of ~3.2 eV at ~390 nm (UV), where the transmittance rapidly increases from zero to a value above 30%, depending on the HCHP treatment time. The oscillations observed above 400 nm are due to the well-known interference effect caused by multiple reflections at the film/substrate and film/air interfaces.

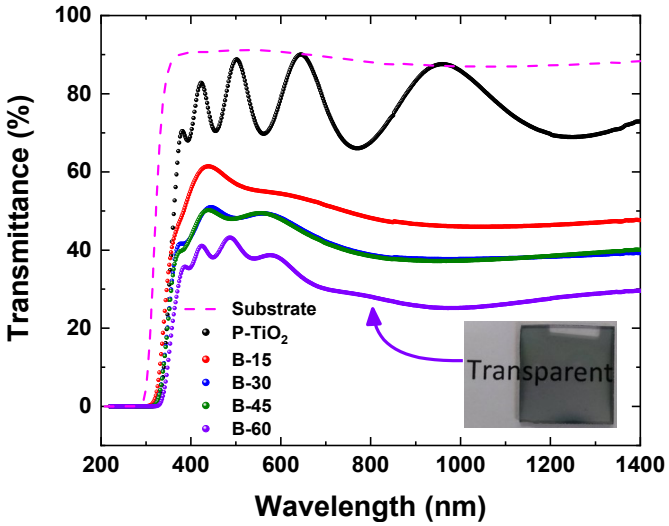

Figure 6. The UV-Vis-NIR transmittance spectra were obtained for glass substrates, both pristine and black TiO_2 thin films, which were hydrogenated using the HCHP process for durations of 15, 30, 45, and 60 min.

The spectra in Figure 6 demonstrate that the absorbance in the visible and NIR regions increases proportionally with the *hydrogen plasma* exposure time. Moreover, even for the longest treatment time, sample B-60, the black TiO_2 thin films remain translucent.

The optical changes observed above are a direct result of a significant increase in $Ti^{3+/2+}$ band states defect density and the increase in tail states breadth between the valence (VB) and conduction (CB) bands for the black TiO_2 [6]. The presence of both phenomena was confirmed by the XPS valence band spectra, as shown in Figure 7 and schematically represented in Figure 8a.

All samples exhibit tail states (TS), denoted as Δ in Figure 7. As the HCHP treatment time increases, the TS breadth tends to expand, displaying a quasi-linear trend with a rate of 6.8×10^{-3} eV min^{-1}, as illustrated in Figure 8b. From Figure 7, a significant increase in $Ti^{3+/2+}$ defect band states can be observed, transitioning from the pristine sample to the 15-min HCHP treated sample, as detailed in Table 3. Furthermore, the similar values obtained for both Ds (TS breadths of 0.67 and 0.65 eV, respectively) and the $Ti^{3+/2+}$ state percentages (Table 3) for samples B-30 and B-45 can account for the comparable light absorption performance observed in the spectrophotometry results (Figure 6).

Consistent with the results discussed in the preceding sections, Fan et al. reported analogous changes concerning the TS in the valence band following the hydrogenation process. The authors attributed the presence of these TS to structural disorder induced in the TiO_2 structure, primarily through the creation of V_o [46]. It is important to emphasize that the existence of a TS with a size of 0.29 eV in the pristine TiO_2 thin film is due to its intrinsic structural defects, as previously mentioned.

Furthermore, the valence band (Figure 7) can be deconvoluted into four peaks centered at 10.3 eV (γ), 7.7 eV (σ), 5.7 eV (π), and 4.5 eV (for the pristine sample), which are attributed to OH groups, π-type molecular orbitals, σ-type molecular orbitals, and nonbonding *O* 2*p* orbitals, respectively [37]. Additionally, another peak centered at 0.8 eV (for the pristine TiO_2) can be fitted to the acquired spectra and is associated with the $Ti^{3+/2+}$ 3*d* states. These

in-gap states, along with the tail states, contribute to narrowing the bandgap and consequently increasing light absorption [47], which is in line with the spectrophotometry results.

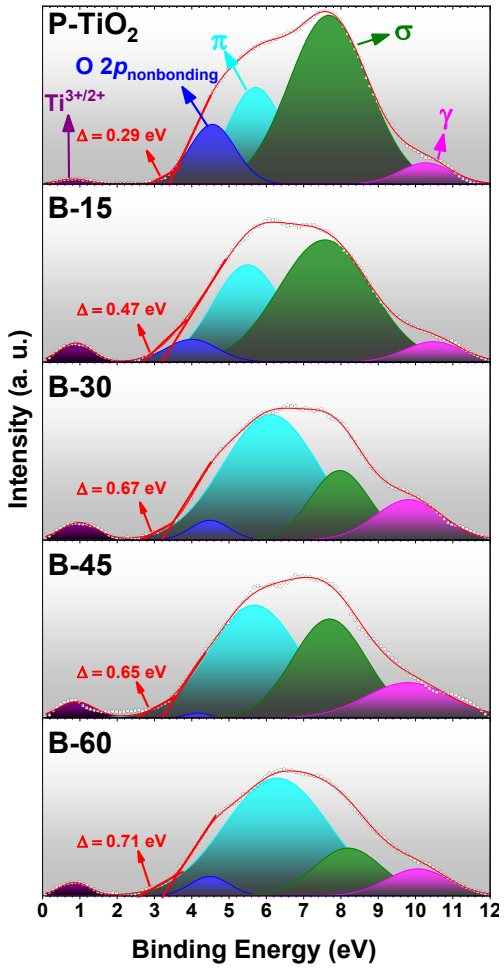

Figure 7. XPS valence band spectra were obtained for both pristine and black TiO_2 thin films subjected to the HCHP process for durations of 15, 30, 45, and 60 min.

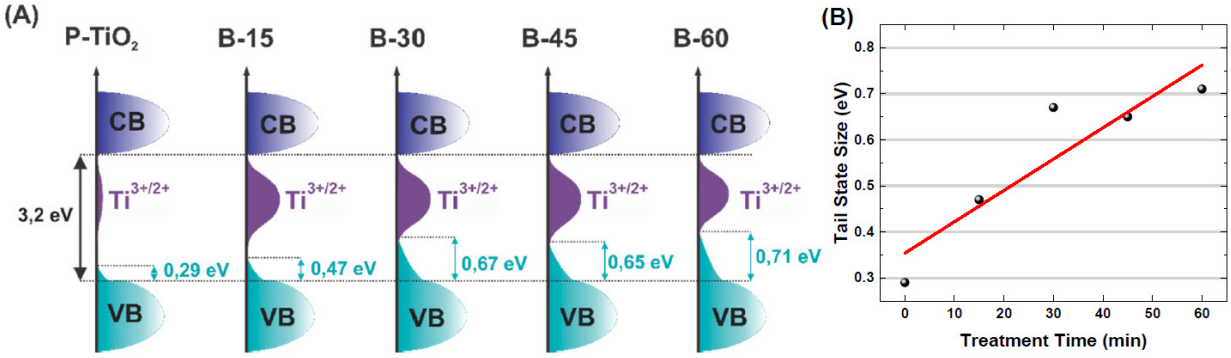

Figure 8. (**A**) Schematic representation of defect $Ti^{3+/2+}$ and tail states occurring between the valence and conduction bands; (**B**) the increase in tail state size as a function of HCHP treatment time, with the red line representing a linear fit.

By analyzing the areas of the deconvoluted fitted peaks, we can quantitatively assess the composition concerning each species and orbitals as the hydrogenation treatment time increases. The percentage area of the γ peak increases at a rate of 0.11% min^{-1}, indicating a rise in the concentration of *OH* groups on the black TiO_2 thin film as the HCHP

process duration increases. Simultaneously, as the concentration of π-type molecular orbitals increases, the σ-type molecular orbitals decrease at the same rate of ~0.7% min^{-1}. From Figure 7, it can be observed that the growth of the π-type molecular orbitals peak contribution was the primary factor resulting in the TS size increase. Furthermore, the concentration of nonbonding O 2*p* orbitals decreases at a rate of −0.14% min^{-1} as the exposure time of the TiO_2 thin films to the *hydrogen plasma* increases, which is consistent with the previously discussed XPS results. These nonbonding O 2*p* orbitals are related to the removal of oxygen atoms from the TiO_2 structure [37].

Moreover, the alterations in the bandgap of black TiO_2 thin films led to changes in their electrical properties. Figure 9 demonstrates a significant sheet resistance reduction of 99.98% after 15 min of hydrogenation, and for longer durations, the sheet resistance of the samples continues to decrease, albeit at a slightly lower rate of −20 (Ω/□) min^{-1}. This enhancement in conductivity can be attributed to the increased concentration of *Ti* suboxides ($Ti^{3+/2+}$) in the black TiO_2 thin films, as they result in an excess of electrons in the electronic states adjacent to the Fermi edge [37,48].

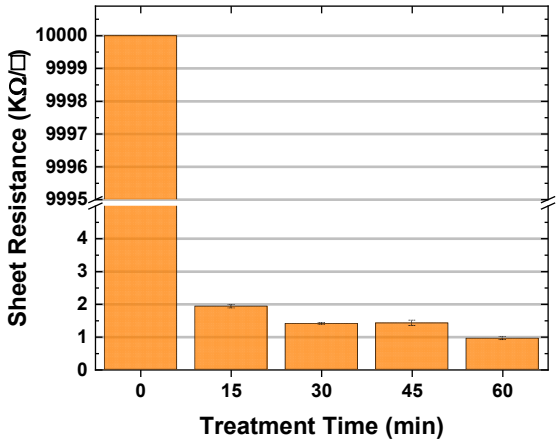

Figure 9. Sheet resistance (in kΩ per square-□) values as the HCHP treatment time increases.

3.6. Photocatalytic Degradation of Methylene Blue Dye

The photoactivity (PA) of pristine TiO_2 and hydrogenated TiO_2, treated for different durations, is compared based on the photodegradation rate of methylene blue (MB) under UV-Visible irradiation, as shown in Figure 10a. It is evident that the pure MB solution displayed negligible photocatalytic activity when exposed to light. In contrast, the photocatalytic activity of the films increased under the test conditions due to hydrogenation treatment, as evidenced by the concentration ratio (C_o/C) of MB plotted against the light irradiation time in the presence of the photocatalysts.

Figure 10a reveals that the B-15 and B-30 samples demonstrated higher photodegradation rates, with around 60% of the MB dye decomposed, while the B-45 and B-60 samples exhibited photodegradation performance at around 45%. However, all black TiO_2 samples displayed superior photocatalytic performance compared to the pristine TiO_2 film, which decomposed only about 25% of MB after 90 min of reaction. The improved photocatalytic performance of the black TiO_2 films can be attributed to the presence of $Ti^{3+/2+}$ interstitials, oxygen vacancies (V_o), and hydroxyl radicals (*OH*) on the film surface. These findings align with the results obtained from XPS analysis.

Although $Ti^{3+/2+}$ and V_o species play a significant role in improving the PA, the formed *OH* groups are the primary oxidative species in photocatalysis reactions, as they exhibit strong performance in the photodecomposition of organic molecules. Moreover, the enhanced surface area of the films may also play a role in improving photocatalytic activity, as it is a crucial factor in enhancing dye degradation, as evidenced by the AFM results.

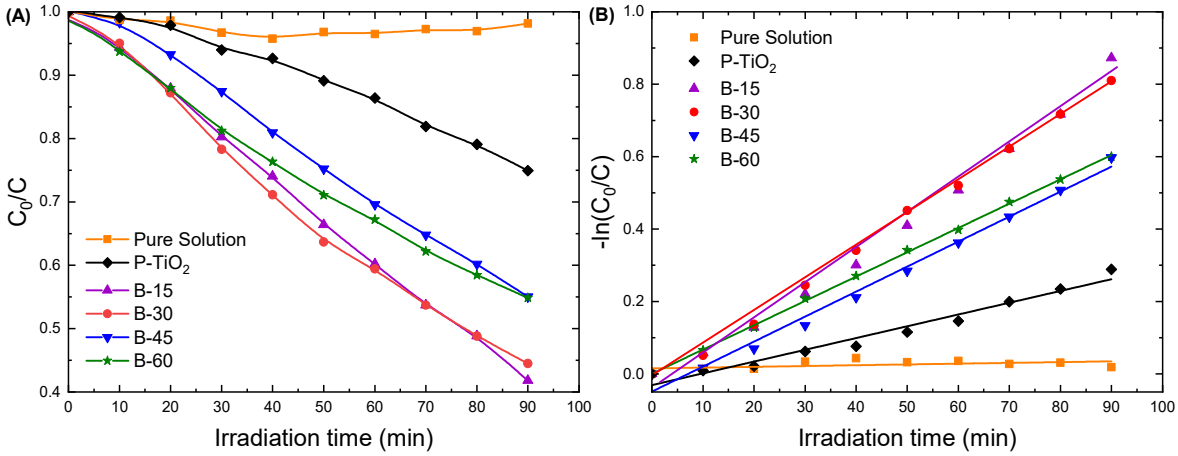

Figure 10. (**A**) MB photodegradation comparison over pristine TiO_2 and black TiO_2 hydrogenated by different conditions under UV light; (**B**) determination of rate of constant via -ln(C_o/C) vs. time plot for photocatalytic degradation of MB system under UV light.

The photodegradation reaction rates of pristine TiO_2, pure solution, and all-black TiO_2 films are compared by plotting $-\ln(C_o/C)$ against hydrogenation irradiation time, as illustrated in Figure 10b. It was observed that the photoactivity of black TiO_2 varies depending on the hydrogenation time, and the PA did not increase consistently with longer durations. When compared to the PA of pristine TiO_2 (2.5×10^{-3} min^{-1}), black TiO_2 films experienced a minimum two-fold increase in photoactivity after hydrogen treatment.

Figure 10b demonstrates that black TiO_2 hydrogenated for 45, 60, 30, and 15 min exhibited significant improvements in photoactivity, in descending order. The corresponding reaction rate constants (k) were 5.1×10^{-3} min^{-1}, 6.7×10^{-3} min^{-1}, 7.1×10^{-3} min^{-1}, and 9.6×10^{-3} min^{-1}, respectively. Prolonged hydrogenation may generate a high concentration of oxygen vacancies (V_o) within the TiO_2 bulk, inducing charge annihilation centers and potentially increasing the electron-hole recombination rate. These factors, combined with the reduction of the thin film surface area, may contribute to the impaired efficiency of photocatalytic degradation.

This can lead to an improvement in visible light absorption while negatively affecting the photocatalytic activity of black TiO_2 nanomaterials, which may explain why the B-15 and B-30 samples demonstrated better results than the others.

4. Conclusions

In conclusion, this study comprehensively highlights how the HCHP treatment influences the transformation of TiO_2 thin films into black TiO_2. The mechanism involves introducing reactive hydrogen species to TiO_2, triggering chemical reactions that create oxygen vacancies and reduce Ti^{4+} oxidation states to $Ti^{3+/2+}$ species. The presence of these species and the induced lattice defects, including titanium suboxides, significantly alter the film's optical and electrical properties.

Notably, this treatment has boosted light absorption by ~30% and conductivity by ~99.98% after 60 min of treatment, ascribed to an increased presence of $Ti^{3+/2+}$ interstitials, oxygen vacancies, and hydroxyl radicals on the film surface. HCHP also results in an expansion of tail states between the valence and conduction bands, facilitating the formation of black TiO_2. A 24% increase in surface area is observed within 15 min of treatment, though this begins to decrease with longer durations. Despite these transformative surface changes, the anatase phase of TiO_2 remains intact, a testament to the treatment's selectivity. This treatment's impact on the material's morphological properties is underscored by a change in surface energy and wettability patterns, hinting at the nuanced influence of HCHP treatment.

Experimental results validate the enhanced photocatalytic performance of the treated samples. Following HCHP treatment, the samples eliminated more than 45% of MB dye, a substantial improvement from the untreated film's approximate 25%.

Overall, these findings underscore the power of the HCHP treatment process to transform the photocatalytic properties of TiO_2 films without disrupting their structural integrity. Future studies should focus on the optimization of the treatment duration to maximize photocatalytic performance, contributing to the development of more efficient photocatalytic materials.

Supplementary Materials: The following supporting information can be downloaded at: https://www.mdpi.com/article/10.3390/plasma6020025/s1.

Author Contributions: Conceptualization, A.G.-J., A.P. and R.P.; methodology, A.G.-J., A.P., M.G., R.P., A.d.S.S. and M.M.; formal analysis, A.G.-J., A.P., B.D., I.H., M.G., W.M., D.L. and M.B.; investigation, A.G.-J., A.P., B.D., I.H., M.G., M.B., D.L., R.P. and A.d.S.S.; resources, M.M., A.d.S.S., D.L. and R.P.; data curation, A.G.-J. and A.P.; writing—original draft preparation, A.G.-J. and A.P.; writing—review and editing, A.G.-J., A.P., M.G., D.L., W.M., M.B., M.M., R.P. and A.d.S.S.; supervision, A.P., A.d.S.S. and R.P.; project administration, A.d.S.S.; funding acquisition, M.M., A.d.S.S., D.L. and R.P. All authors have read and agreed to the published version of the manuscript.

Funding: This research was funded by CAPES, CNPq and FAPESP (grant number 2018-6/159754, 2018-5/307199, 2012-9/201050, 2010-8/555.686, 2012-8/470820 and 2015/06241-5).

Institutional Review Board Statement: Not applicable.

Informed Consent Statement: Not applicable.

Data Availability Statement: Not applicable.

Acknowledgments: The authors thank the Associated Laboratory of Sensors and Materials–LABAS of the National Institute of Space Research–INPE, Brazil, for the XPS and FEG-SEM analysis and the Institute of Advanced Studies (IEAv)–Photonics Division (EFO), Brazil, for the spectrophotometry measurements.

Conflicts of Interest: The authors declare no conflict of interest.

References

1. Solak, E.K.; Irmak, E. Advances in organic photovoltaic cells: A comprehensive review of materials, technologies, and performance. *RSC Adv.* **2023**, *19*, 12244–12269. [CrossRef]
2. Querebillo, C.J. A Review on Nano Ti-Based Oxides for Dark and Photocatalysis: From Photoinduced Processes to Bioimplant Applications. *Nanomaterials* **2023**, *13*, 982. [CrossRef]
3. Wang, Y.; Suzuki, H.; Xie, J.; Tomita, O.; Martin, D.J.; Higashi, M.; Kong, D.; Abe, R.; Tang, J. Mimicking Natural Photosynthesis: Solar to Renewable H_2 Fuel Synthesis by Z-Scheme Water Splitting Systems. *Chem. Rev.* **2018**, *118*, 5201–5241. [CrossRef] [PubMed]
4. Pessoa, R.S.; Fraga, M.A.; Santos, L.V.; Massi, M.; Maciel, H.S. Nanostructured Thin Films Based on TiO_2 and/or SiC for Use in Photoelectrochemical Cells: A Review of the Material Characteristics, Synthesis and Recent Applications. *Mater. Sci. Semicond. Process.* **2015**, *29*, 56–68. [CrossRef]
5. Zhang, X.; Xiao, J.; Peng, C.; Xiang, Y.; Chen, H. Enhanced Photocatalytic Hydrogen Production over Conjugated Polymer/Black TiO_2 Hybrid: The Impact of Constructing Active Defect States. *Appl. Surf. Sci.* **2019**, *465*, 288–296. [CrossRef]
6. Chen, X.; Liu, L.; Yu, P.Y.; Mao, S.S. Increasing Solar Absorption for Photocatalysis with Black Hydrogenated Titanium Dioxide Nanocrystals. *Science* **2011**, *331*, 746–750. [CrossRef]
7. Liu, G.; Wang, L.; Yang, H.G.; Cheng, H.M.; Lu, G.Q. Titania-Based Photocatalysts—Crystal Growth, Doping and Heterostructuring. *J. Mater. Chem.* **2010**, *20*, 831–843. [CrossRef]
8. Nair, R.V.; Gayathri, P.K.; Gummaluri, V.S.; Nambissan, P.M.G.; Vijayan, C. Large Bandgap Narrowing in Rutile TiO_2 Aimed towards Visible Light Applications and Its Correlation with Vacancy-Type Defects History and Transformation. *J. Phys. D Appl. Phys.* **2018**, *51*, 045107. [CrossRef]
9. Xu, J.; Huang, J.; Zhang, S.; Hong, Z.; Huang, F. Understanding the Surface Reduction of Nano Rutile and Anatase: Selective Breaking of Ti-O Bonds. *Mater. Res. Bull.* **2020**, *121*, 110617. [CrossRef]
10. Ullattil, S.G.; Narendranath, S.B.; Pillai, S.C.; Periyat, P. Black TiO_2 Nanomaterials: A Review of Recent Advances. *Chem. Eng. J.* **2018**, *343*, 708–736. [CrossRef]

11. Godoy, A., Jr.; Pereira, A.; Gomes, M.; Fraga, M.; Pessoa, R.; Leite, D.; Petraconi, G.; Nogueira, A.; Wender, H.; Miyakawa, W.; et al. Black TiO_2 Thin Films Production Using Hollow Cathode Hydrogen Plasma Treatment: Synthesis, Material Characteristics and Photocatalytic Activity. *Catalysts* **2020**, *10*, 282. [CrossRef]
12. Nair, P.R.; Ramirez, C.R.S.; Pinilla, M.A.G.; Krishnan, B.; Avellaneda, D.A.; Pelaes, R.F.C.; Shaji, S. Black titanium dioxide nanocolloids by laser irradiation in liquids for visible light photo-catalytic/electrochemical applications. *Appl. Surf. Sci.* **2023**, *623*, 157096. [CrossRef]
13. Hu, B.; Liang, C.-H.; Yang, F.; Chen, J.; Jin, W.; Xing, H.; Cai, L.; Yang, S.; Liu, K.Z.; Kleyn, A.W.; et al. TiO_2 Powder Modified by Plasma Afterglow: A Correlation between Active Species, Microstructure, and Optical Properties. *Mater. Lett.* **2020**, *268*, 127577. [CrossRef]
14. Luminita, A.; Alexandru, E. Black TiO_2 Synthesis by Chemical Reduction Methods for Photocatalysis Applications. *Front. Chem.* **2020**, *8*, 565489. [CrossRef]
15. Jian, J.; Sun, Y.; Chen, F.; Wu, R.; Wei, S. Black and Yellow Anatase Titania Formed by (H,N)-Doping: Strong Visible-Light Absorption and Enhanced Visible-Light Photocatalysis. *Dalt. Trans.* **2014**, *44*, 1534–1538. [CrossRef]
16. Naldoni, A.; Allieta, M.; Santangelo, S.; Marelli, M.; Fabbri, F.; Cappelli, S.; Bianchi, C.L.; Psaro, R.; Dal Santo, V. Effect of Nature and Location of Defects on Bandgap Narrowing in Black TiO_2 Nanoparticles. *J. Am. Chem. Soc.* **2012**, *134*, 7600–7603. [CrossRef]
17. Zhao, D.; Xu, B.; Yang, J.; Wu, J.; Zhai, W.; Yang, B.; Liu, M. Rapid Preparation of TiO_{2-x} and Its Photocatalytic Oxidation for Arsenic Adsorption under Visible Light. *Langmuir* **2020**, *36*, 3853–3861. [CrossRef]
18. Wang, Z.; Yang, C.; Lin, T.; Yin, H.; Chen, P.; Wan, D.; Xu, F.; Huang, F.; Lin, J.; Xie, X.; et al. H-Doped Black Titania with Very High Solar Absorption and Excellent Photocatalysis Enhanced by Localized Surface Plasmon Resonance. *Adv. Funct. Mater.* **2013**, *23*, 5444–5450. [CrossRef]
19. Li, B.; Zhao, Z.; Zhou, Q.; Meng, B.; Meng, X.; Qiu, J. Highly Efficient Low-Temperature Plasma-Assisted Modification of TiO_2 Nanosheets with Exposed {001} Facets for Enhanced Visible-Light Photocatalytic Activity. *Chem. A Eur. J.* **2014**, *20*, 14763–14770. [CrossRef]
20. Hu, L.; Song, X.; Shan, X.; Zhao, X.; Guo, F.; Xiao, P. Visible Light-Activated Self-Recovery Hydrophobic CeO_2/Black TiO_2 Coating Prepared Using Air Plasma Spraying. ACS Appl. *Mater. Interfaces* **2019**, *11*, 37209–37215. [CrossRef]
21. Zhai, M.; Liu, Y.; Huang, J.; Wang, Y.; Chen, K.; Fu, Y.; Li, H. Efficient Suspension Plasma Spray Fabrication of Black Titanium Dioxide Coatings with Visible Light Absorption Performances. *Ceram. Int.* **2019**, *45*, 930–935. [CrossRef]
22. Pylnev, M.; Wong, M.S. Comparative Study of Photocatalytic Deactivation of Pure and Black Titania Thin Films. *J. Photochem. Photobiol. A Chem.* **2019**, *378*, 125–130. [CrossRef]
23. Islam, S.Z.; Reed, A.; Nagpure, S.; Wanninayake, N.; Browning, J.F.; Strzalka, J.; Kim, D.Y.; Rankin, S.E. Hydrogen Incorporation by Plasma Treatment Gives Mesoporous Black TiO_2 Thin Films with Visible Photoelectrochemical Water Oxidation Activity. *Microporous Mesoporous Mater.* **2018**, *261*, 35–43. [CrossRef]
24. Zhang, W.; Gu, J.; Li, K.; Zhao, J.; Ma, H.; Wu, C.; Zhang, C.; Xie, Y.; Yang, F.; Zheng, X. A Hydrogenated Black TiO_2 Coating with Excellent Effects for Photothermal Therapy of Bone Tumor and Bone Regeneration. *Mater. Sci. Eng. C* **2019**, *102*, 458–470. [CrossRef] [PubMed]
25. Yan, Y.; Hao, B.; Wang, D.; Chen, G.; Markweg, E.; Albrecht, A.; Schaaf, P. Understanding the Fast Lithium Storage Performance of Hydrogenated TiO_2 Nanoparticles. *J. Mater. Chem. A* **2013**, *1*, 14507. [CrossRef]
26. Teng, F.; Li, M.; Gao, C.; Zhang, G.; Zhang, P.; Wang, Y.; Chen, L.; Xie, E. Preparation of Black TiO_2 by Hydrogen Plasma Assisted Chemical Vapor Deposition and Its Photocatalytic Activity. *Appl. Catal. B Environ.* **2014**, *148–149*, 339–343. [CrossRef]
27. Ren, W.; Yan, Y.; Zeng, L.; Shi, Z.; Gong, A.; Schaaf, P.; Wang, D.; Zhao, J.; Zou, B.; Yu, H.; et al. A Near Infrared Light Triggered Hydrogenated Black TiO_2 for Cancer Photothermal Therapy. *Adv. Healthc. Mater.* **2015**, *4*, 1526–1536. [CrossRef]
28. Godoy, A.; Carlucci, F.G.; Leite, D.M.G.; Miyakawa, W.; Pereira, A.L.J.; Massi, M.; da Silva Sobrinho, A.S. Plasma Nanotexturing of Amorphous Carbon Films by Reactive Ion Etching. *Surf. Coatings Technol.* **2018**, *354*, 153–160. [CrossRef]
29. Duarte, D.A.; Massi, M.; Da Silva Sobrinho, A.S. Comparison between Conventional and Hollow Cathode Magnetron Sputtering Systems on the Growing of Titanium Dioxide Thin Films: A Correlation between the Gas Discharge and Film Formation. *EPJ Appl. Phys.* **2011**, *54*, 20801. [CrossRef]
30. Degen, T.; Sadki, M.; Bron, E.; König, U.; Nénert, G. The HighScore Suite. *Powder Diffr.* **2014**, *29*, S13–S18. [CrossRef]
31. Axis, K. *Peak Fitting in XPS*; Casa XPS: Pasadena, CA, USA, 2006.
32. Gomes, L.E.; Da Silva, M.F.; Gonçalves, R.V.; Machado, G.; Alcantara, G.B.; Caires, A.R.L.; Wender, H. Synthesis and Visible-Light-Driven Photocatalytic Activity of Ta^{4+} Self-Doped Gray Ta_2O_5 Nanoparticles. *J. Phys. Chem. C* **2018**, *122*, 6014–6025. [CrossRef]
33. Nogueira, A.C.; Gomes, L.E.; Ferencz, J.A.P.; Rodrigues, J.E.F.S.; Gonçalves, R.V.; Wender, H. Improved Visible Light Photoactivity of $CuBi_2O_4$/CuO Heterojunctions for Photodegradation of Methylene Blue and Metronidazole. *J. Phys. Chem. C* **2019**, *123*, 25680–25690. [CrossRef]
34. Baik, S.J.; Jang, J.H.; Lee, C.H.; Cho, W.Y.; Lim, K.S. Highly Textured and Conductive Undoped ZnO Film Using Hydrogen Post-Treatment. Appl. *Phys. Lett.* **1997**, *70*, 3516–3518. [CrossRef]
35. Wang, F.-H.; Chao, J.-C.; Liu, H.-W.; Liu, F.-J. Physical Properties of TiO_2-Doped Zinc Oxide Thin Films: Influence of Plasma Treatment in H_2 and/or Ar Gas Ambient. *Vacuum* **2017**, *140*, 155–160. [CrossRef]

36. Han, J.; Cheng, Y.; Tu, W.; Zhan, T.-Y.; Cheng, Y. The Black and White Coatings on Ti-6Al-4V Alloy or Pure Titanium by Plasma Electrolytic Oxidation in Concentrated Silicate Electrolyte. *Appl. Surf. Sci.* **2018**, *428*, 684–697. [CrossRef]
37. Hannula, M.; Ali-Löytty, H.; Lahtonen, K.; Sarlin, E.; Saari, J.; Valden, M. Improved Stability of Atomic Layer Deposited Amorphous TiO_2 Photoelectrode Coatings by Thermally Induced Oxygen Defects. *Chem. Mater.* **2018**, *30*, 1199–1208. [CrossRef] [PubMed]
38. Lepcha, A.; Maccato, C.; Mettenbörger, A.; Andreu, T.; Mayrhofer, L.; Walter, M.; Olthof, S.; Ruoko, T.-P.; Klein, A.; Moseler, M.; et al. Electrospun Black Titania Nanofibers: Influence of Hydrogen Plasma-Induced Disorder on the Electronic Structure and Photoelectrochemical Performance. *J. Phys. Chem. C* **2015**, *119*, 18835–18842. [CrossRef]
39. Liu, X.; Xing, Z.; Zhang, H.; Wang, W.; Zhang, Y.; Li, Z.; Wu, X.; Yu, X.; Zhou, W. Fabrication of 3D Mesoporous Black $TiO_2/MoS_2/TiO_2$ Nanosheets for Visible-Light-Driven Photocatalysis. *ChemSusChem* **2016**, *9*, 1118–1124. [CrossRef]
40. Panomsuwan, G.; Watthanaphanit, A.; Ishizaki, T.; Saito, N. Water-Plasma-Assisted Synthesis of Black Titania Spheres with Efficient Visible-Light Photocatalytic Activity. *Phys. Chem. Chem. Phys.* **2015**, *17*, 13794–13799. [CrossRef]
41. Kibasomba, P.M.; Dhlamini, S.; Maaza, M.; Liu, C.P.; Rashad, M.M.; Rayan, D.A.; Mwakikunga, B.W. Strain and Grain Size of TiO_2 Nanoparticles from TEM, Raman Spectroscopy and XRD: The Revisiting of the Williamson-Hall Plot Method. *Results Phys.* **2018**, *9*, 628–635. [CrossRef]
42. Tudu, B.K.; Gupta, V.; Kumar, A.; Sinhamahapatra, A. Freshwater Production via Efficient Oil-Water Separation and Solar-Assisted Water Evaporation Using Black Titanium Oxide Nanoparticles. *J. Colloid Interface Sci.* **2020**, *566*, 183–193. [CrossRef] [PubMed]
43. Wang, G.; Wang, H.; Ling, Y.; Tang, Y.; Yang, X.; Fitzmorris, R.C.; Wang, C.; Zhang, J.Z.; Li, Y. Hydrogen-Treated TiO_2 Nanowire Arrays for Photoelectrochemical Water Splitting. *Nano Lett.* **2011**, *11*, 3026–3033. [CrossRef] [PubMed]
44. Wang, X.; Ma, B.; Xue, J.; Wu, J.; Chang, J.; Wu, C. Defective Black Nano-Titania Thermogels for Cutaneous Tumor-Induced Therapy and Healing. *Nano Lett.* **2019**, *19*, 2138–2147. [CrossRef] [PubMed]
45. Saied, S.; Sullivan, J.; Choudhury, T.; Pearce, C. A Comparison of Ion and Fast Atom Beam Reduction in TiO_2. *Vacuum* **1988**, *38*, 917–922. [CrossRef]
46. Fan, C.; Chen, C.; Wang, J.; Fu, X.; Ren, Z.; Qian, G.; Wang, Z. Black Hydroxylated Titanium Dioxide Prepared via Ultrasonication with Enhanced Photocatalytic Activity. *Sci. Rep.* **2015**, *5*, srep11712. [CrossRef]
47. Chen, X.; Burda, C. The Electronic Origin of the Visible-Light Absorption Properties of C-, N- and S-Doped TiO_2 Nanomaterials. *J. Am. Chem. Soc.* **2008**, *130*, 5018–5019. [CrossRef]
48. Di Valentin, C.; Pacchioni, G.; Selloni, A. Reduced and N-Type Doped TiO_2: Nature of Ti^{3+} Species. *J. Phys. Chem. C* **2009**, *113*, 20543–20552. [CrossRef]